NASA TECHNICAL MEMORANDUM

NASA TM X-3499

NASA TM X-3499

GRAPHICAL METHOD FOR PREDICTING LIFE OF A ROCKET THRUST CHAMBER WITH HALF-HARD ZIRCONIUM COPPER LINER AND ELECTROFORMED NICKEL CLOSEOUT

Harold J. Kasper

Lewis Research Center

Cleveland, Ohio 44135

NATIONAL AERONAUTICS AND SPACE ADMINISTRATION • WASHINGTON, D. C. • MARCH 1977

1. Report No. NASA TM X-3499	2. Government Accession No.	3. Recipient's Catalog No.
4. Title and Subtitle GRAPHICAL METHOD FOR PREDICTING LIFE OF A ROCKET THRUST CHAMBER WITH HALF-HARD ZIRCONIUM-COPPER LINER AND ELECTROFORMED NICKEL CLOSEOUT		5. Report Date March 1977 6. Performing Organization Code
7. Author(s) Harold J. Kasper		8. Performing Organization Report No. E-8971 10. Work Unit No. 506-21
9. Performing Organization Name and Address Lewis Research Center National Aeronautics and Space Administration Cleveland, Ohio 44135		11. Contract or Grant No. 13. Type of Report and Period Covered Technical Memorandum
12. Sponsoring Agency Name and Address National Aeronautics and Space Administration Washington, D.C. 20546		14. Sponsoring Agency Code
15. Supplementary Notes		

16. Abstract

A simple method for estimating the life of a regeneratively cooled rocket thrust chamber has been developed and is based on the hot-gas wall temperature and the temperature difference between the hot-gas wall and the outside surface of the closeout. This method permits a quick estimate of the life of a thrust chamber when design changes or test-cycle variations are considered. Strain range and life are presented graphically as functions of these temperature parameters for a typical high-performance rocket thrust chamber with a half-hard zirconium-copper liner and an electroformed nickel closeout.

17. Key Words (Suggested by Author(s))	18. Distribution Statement
Copper alloys; Fatigue life; Graphs (charts); Rocket nozzles; Spacecraft propulsion; Thermal fatigue; Thrust chambers	Unclassified - unlimited STAR Category 20

19. Security Classif. (of this report)	20. Security Classif. (of this page)	21. No. of Pages	22. Price*
Unclassified	Unclassified	28	A03

* For sale by the National Technical Information Service, Springfield, Virginia 22161

GRAPHICAL METHOD FOR PREDICTING LIFE OF A ROCKET THRUST CHAMBER WITH HALF-HARD ZIRCONIUM COPPER LINER AND ELECTROFORMED NICKEL CLOSEOUT

by Harold J. Kasper

Lewis Research Center

SUMMARY

A simple method for estimating the life of a regeneratively cooled rocket thrust chamber has been developed and is based on the hot-gas wall temperature and the temperature difference between the hot-gas wall and the outside surface of the closeout. This method permits a quick estimate of the life of a thrust chamber when design changes or test-cycle variations are considered. Strain range and life are presented graphically as functions of these temperature parameters for a typical high-performance rocket thrust chamber with a half-hard zirconium copper liner and an electroformed nickel closeout.

INTRODUCTION

The Space Shuttle has introduced many new design requirements for rocket thrust chambers. One of these is reusability, which has not been a major design requirement in the past. Now that more emphasis is being put on economy in space endeavors, the need for reusability is apparent. In order to minimize engine weight and volume requirements, future rocket engines may be required to operate at chamber pressures well above those of present engines. Consequently, the heat flux in the throat region will increase considerably.

One of the chief concerns in the design of a reusable regeneratively cooled thrust chamber is the fatigue life of the thrust chamber liner. The increased heat flux in the throat region, which is a result of higher chamber pressures, contributes significantly to the complexity of this design problem. The large temperature differences that occur between the inner wall and the outer shell during engine operation usually create plastic strains that have a major effect on thrust chamber life. During engine startup when the

inner wall is hotter than the outer shell, large compressive plastic strains are created near the inner wall. When the engine is shut down and if the coolant flow continues in the cooling channels, which is typical for a fatigue-life test cycle, the inner wall becomes cooler than the outside shell and tensile strains occur near the inner wall. The range between these strains is referred to as the total strain range. There is an inverse relationship between this total strain range and cyclic life: as total strain range increases, cyclic life decreases. Therefore, in order to design an engine for a predetermined life, it is necessary to predict the cyclic strains as accurately as possible.

A program has been initiated at the Lewis Research Center to study the effects of thrust chamber liner materials, coatings, and designs on chamber life. Low strength, high conductivity materials in particular are being studied because the theoretical coolant wall thickness required by the higher strength, low conductivity materials to transfer the increased heat load at acceptable material temperatures is too small to sustain the coolant pressure load. Thrust chambers employing the various materials are fabricated and then subjected to a cyclic combustion environment until failure occurs. In conjunction with this, the cyclic lives of these thrust chambers are predicted so that the analytical methods can be verified. During the course of the test program, it is desirable to have a simple method of predicting life based on measured wall temperatures so that if the test cycle conditions are adjusted, the corresponding effect on life can be quickly estimated.

The purpose of this report is to present a simple graphical method of predicting the life of a typical test thrust chamber based on the hot-gas wall temperature and the temperature difference between the hot-gas wall and the closeout outside surface. The graphs are for a test thrust chamber with a 6.6-centimeter (2.6-in.) diameter throat, a half-hard zirconium copper liner, and an electroformed nickel closeout. The propellants used are hydrogen and oxygen at an oxidant-fuel ratio of 6.0 and a chamber pressure of 4.137 meganewtons per square meter (600 psia). A more detailed description of the chamber is given in reference 1. The method of analysis and the resulting graphs are presented herein.

ANALYTICAL METHOD

The conventional analytical approach to life prediction of a regeneratively cooled thrust chamber such as the one shown in figure 1 includes a computer thermal analysis and a computer structural analysis of the throat section. The throat section is normally chosen for the life analysis because the high heat flux that occurs here generally produces the maximum strain. Temperatures obtained from the thermal analysis program are input to the structural analysis program as loading conditions along with the thrust load and the pressure loads.

The thermal map required for the structural analysis is usually generated with a thermal analyzer computer program such as SINDA (ref. 2). Input to this program requires hot-gas and coolant wall heat-transfer boundary conditions as functions of time. Temperatures such as those in figure 2 are output for the selected cross section at arbitrarily selected time intervals. The numbers appearing on the model in figure 2 identify the locations at which temperatures are calculated, and the accompanying table lists typical corresponding temperatures. Figure 3 shows the throat section structural model and the identifying element numbers for the structural finite-element analysis. The temperature map required by the structural analysis program is based on the structural model; that is, a temperature is required at the center of each structural element of figure 3. Figure 2 shows that the SINDA thermal map provides 68 internal temperatures and 23 boundary temperatures. Therefore, the SINDA temperature that is nearest to the center of each of the 34 structural elements is selected as the temperature of that element. In some instances, two temperatures near an element center are averaged. A revised temperature map corresponding to the structural element center locations is shown in figure 4.

Although the SINDA program provides temperatures as a function of time, only two times are selected for the structural analysis. These times correspond to the points of maximum temperature difference ΔT between the hot-gas wall and the closeout outside surface during the start transient and during the shutdown transient of the firing cycle. Generally, this is when the maximum compressive and tensile strains occur. During the start transient, large compressive plastic strains are induced in the copper liner. This is a result of the hot copper liner being restricted in its thermal growth by the cooler nickel closeout. The magnitude of these strains is related to ΔT. During the test cycle shutdown transient, tensile strains are induced in the copper liner because the coolant is allowed to flow continuously as the engine is started and stopped, which allows the closeout to acquire a higher temperature than the liner. The relationship between coolant flow, cyclic ΔT and chamber pressure is shown in the two cycle schematics of figure 5. Both firing cycles were used during the test program and each produced approximately the same temperature differences during the start and shutdown transients.

Once the thermal maps are obtained, the fatigue-life strain range of each element is calculated by using the thermal map for the start transient peak ΔT as input to the three-dimensional finite-element program RETSCP (refs. 4 and 5). Total strain and residual strain (plastic strain) are determined for each element. Residual strains are then input along with the shutdown transient peak ΔT thermal map, and total strains for the combined loading are provided as output. The strain range for these loading conditions is obtained from a typical stress-strain hysteresis loop (fig. 6). During the start transient, the total strain ϵ_{tot}^{H} in the critical element of the hot liner includes plastic deformation. During the shutdown transient, the state of strain in the critical element reverses along the elastic-plastic line until a total strain of ϵ_{tot}^{C} is achieved. In the

process of this reversal the strain state passes through a zero stress point that corresponds with the residual plastic strain ϵ_p^H. The strain range is the strain between the peak strain points of the loop and is given by

$$\text{Strain range} = \Delta\epsilon = \epsilon_{tot}^H + \epsilon_{tot}^c - \epsilon_p^H \tag{1}$$

Thrust chamber life is then predicted from a curve that relates strain range and cycles to fracture for the liner material. Such a curve for half-hard zirconium copper was taken from reference 6 and is shown in figure 7.

GRAPHICAL METHOD

The graphical method eliminates the thermal and structural computer analyses and allows the strain range and hence life to be determined from the hot-gas wall temperature and the temperature difference ΔT. The method used to construct these graphs and their application follows.

Thermal Map Development

In order to produce a family of curves that show the relationship between strain, hot-gas wall temperature, and temperature difference, it is necessary to compute a thermal map for each point needed to plot a curve. This becomes a lengthy procedure when using SINDA because input boundary conditions must be repeatedly adjusted until the desired temperatures are output at the hot-gas wall and the closeout outside surface. Therefore, temperature equations and weighting factors were used in place of SINDA to generate the required thermal maps.

The temperature equation for the critical time during the start transient was taken from reference 3 and modified. This resulted in

$$T = (T_i - T_o)\left(\frac{\ln \frac{r_o}{r}}{\ln \frac{r_o}{r_i}}\right)^2 + T_o \tag{2}$$

where

T temperature at radius r

T_i hot-gas wall temperature

T_o closeout outside surface temperature

r_o outside radius

r variable radius

r_i inside radius

This equation provides a radial temperature distribution only and does not account for any circumferential variation. Therefore, the temperature calculated with this equation for each row of structural elements was considered as an average temperature for that row.

To account for the circumferential variation in temperature, a weighting factor was applied to the temperature calculated from equation (2). The weighting factors were determined from SINDA thermal maps by calculating the ratio of each element temperature to the corresponding average temperature for that element row. For example, referring to figure 4, the average temperature for the element 30 to element 34 row is 728 K (1311° R). The weighting factor for element 30 is the ratio of 749 K (1348° R) to 728 K (1311° R) or 1.028. This was done for each structural element of the revised SINDA thermal maps associated with the cases of table I. (These cases were analyzed during the development of the final test cycle.) Hence, there were five weighting factors for each element based on the five thermal maps. The final weighting factor for each element was taken as the average of these five factors.

In examining the SINDA thermal maps, it was observed that the circumferential temperature variation was approximately the same for the corresponding rows of the different cases. Therefore, it was felt that the average of the circumferential weighting factors would adequately account for the circumferential temperature variation of all cases. Furthermore, the radial temperature gradient is usually predominant in influencing the thermal strain throughout the cross section. The weighting factors and the average weighting factor for each element are given in table II.

To calculate a thermal map for a particular hot-gas wall temperature and temperature difference, the midpoint temperature for the element row was calculated with equation (2). This value was multiplied by the weighting factor for each element in that row to obtain the element temperature. This procedure was executed for the various element rows appearing in the structural model.

The procedure used to generate the maximum strain thermal map for the shutdown transient was the same except for the radial temperature equation. Two equations were used in place of equation (2). They were

$$T = T_i \tag{3}$$

where $3.30 \leq r < 3.38$ centimeters ($1.300 \leq r < 1.3325$ in.), and

$$T = (T_i - T_o)\left(\frac{\ln \frac{r_o}{r}}{\ln \frac{r_o}{r_i}}\right)^{0.75} + T_o \qquad (4)$$

where $3.38 \leq r \leq 4.18$ centimeters ($1.3325 \leq r \leq 1.6440$ in.) and $r_i = 3.38$ centimeters (1.3325 in.).

The temperature variation between the hot-gas surface ($r = 3.30$ cm; 1.300 in.) and the coolant surface ($r = 3.38$ cm; 1.3325 in.) at the time of the shutdown maximum temperature difference was small. Therefore, all element temperatures within these boundaries were considered to be equal to the hot-gas wall temperature (eq. (3)), and the inside radius of equation (4) was taken as 3.38 centimeter (1.3325 in.). The weighting factors for the shutdown transient temperatures are tabulated in table III. A discussion of the accuracy of the equation-factor method for calculating thermal maps is included in the appendix.

Graph Construction

Structural computer runs were made using start transient thermal maps derived from the equation-factor method with various inside and outside temperatures. Maximum strain was plotted as a function of ΔT and hot-gas wall temperature in figure 8. Notice that the upper limit of each curve occurs at a ΔT equal to the hot-gas wall temperature, which corresponds to an outside temperature of 0 K (0° R). Separate shutdown transient structural computer runs were made independent of the start transient runs using equation calculated thermal maps and neglecting residual strains. Maximum strains for the shutdown transient runs are plotted in figure 9. The ΔT values along the abscissa of the graph in this figure are shown as negative values. This is because the chamber outside surface temperature is greater than the hot-gas wall temperature during shutdown and because the previous definition of ΔT has been maintained ($\Delta T = T_i - T_o$). To estimate the strain range, the strain corresponding to the start transient ΔT and the hot-gas wall temperature is read from figure 8 and the strain corresponding to the shutdown transient ΔT and the hot-gas wall temperature is read from figure 9. The two strains are added to obtain the estimated strain range.

The graph in figure 10, which relates cycle life to ΔT and hot-gas wall temperature, is a composite of figures 7 to 9. Strain values corresponding to various ΔT values and hot-gas wall temperatures were taken from figure 8 and increased by

10 percent to account for the small shutdown transient strain that is added to the start transient strain to obtain the strain range. The shutdown transient strain is normally considerably smaller than the start transient strain because the maximum shutdown transient ΔT is much less severe. Cycle lives corresponding to the increased start transient strains were taken from figure 7 and plotted against the corresponding ΔT values and along corresponding constant hot-gas wall temperature lines. Hence, an estimated cycle life can be determined directly from ΔT and the hot-gas wall temperature.

Application of Graphs

As an example of the application of the graphs, a start transient hot-gas wall temperature of 833 K (1500° R) and a ΔT of 667 K (1200° R) are assumed. A maximum start transient strain of 2.38 percent is obtained from figure 8. A maximum shutdown transient strain of 0.25 percent, corresponding to an assumed hot-gas wall temperature of 111 K (200° R) and a ΔT of -167° C (-300° F) is obtained from figure 9. The strain range is then calculated by adding these two strains, which results in a strain range of 2.63 percent. Using this value and figure 7 results in an expected fatigue life of 770 cycles. An expected fatigue life of 770 cycles is also obtained from figure 10 with the same start transient temperatures that were assumed previously.

RESULTS AND DISCUSSION

In an effort to evaluate the effect of neglecting the residual strains in the graphical method, a structural analysis that included the residual strains was performed. The thermal map corresponding to the start transient ΔT and hot-gas wall temperature of the example given in the previous section was input to the structural program. The residual strains from this analysis were then input along with the shutdown transient ΔT and hot-gas wall temperature of the same example. The resulting strain range was 2.44 percent, while that obtained from the graphical method was 2.63 percent. Hence, the inclusion of residual strains had a little effect on the total strain range. Furthermore, the expected fatigue life for the 2.44 percent strain range was 900 cycles and for the 2.63 percent strain range, 770 cycles. Therefore, the graphical method is conservative because the larger strain range obtained by adding the graphical values resulted in a shorter expected life.

Table I lists the cycle conditions of five theoretical firing cycles used in the development of the test program firing cycle. Table IV shows maximum strain range values for these five cases. The values in the second column were obtained with SINDA generated thermal maps and RETSCP and have residual strains included. Also shown are

maximum strain range values obtained from figures 8 and 9. Although the particular location of the maximum strain range varied slightly, it was always within the 0.09 centimeter (0.035 in.) inside annulus of the chamber where the strain ranges were generally much larger than those in other locations. This typical area of large strain ranges can be seen in the strain range distribution of case 5 (fig. 11). The strain ranges obtained from the graphs are larger than those with the residual strains included in four of the five cases as seen in table IV. It was again concluded from this and the fact that life decreases with increasing strain range, that the graphical method will normally give more conservative life predictions than those obtained with the more rigorous method.

Figure 10 shows that cycle life decreases with increasing ΔT and increasing gas wall temperature. Also, at the lower ΔT values (below approximately 555 K (1000° R)) and the lower hot-gas wall temperatures (below approximately 722 K; 1300° R), it appears that an equal reduction in either of these has about the same effect on life. At the higher ΔT values and the higher hot-gas wall temperatures, the slopes of the curves decrease and a reduction in ΔT seems to have less of an effect on increasing life than an equivalent decrease in the hot-gas wall temperature. This is probably due to the material life curve. At the lower strain ranges (below approximately 2%), which corresponds to the lower ΔT values and the lower hot-gas wall temperatures, cycle life increases more rapidly than above 2 percent for an equivalent change in strain range.

CONCLUDING REMARKS

A simple method for predicting the life of a regeneratively cooled thrust chamber with a half-hard zirconium copper liner and a nickel closeout has been presented. Graphs that relate strain range and life to the hot-gas wall temperature and the temperature difference between the hot-gas wall and the closeout outside surface were prepared by substituting temperature equations for the computer analyzer and by neglecting the residual strains in the structural analysis. The accuracy of the graphs was checked by comparing results obtained from the graphs with those obtained from the more sophisticated computer analysis, which employed SINDA and included residual strains in the structural analysis. Since the results from the two methods were fairly close, it may be concluded that figures 7 to 10 are satisfactory for quick strain range and life estimates of thrust chambers similar to those being tested at Lewis.

Although the simplified analysis is for a half-hard zirconium copper liner and a nickel closeout, it should be possible to estimate strain ranges and lives of other liner materials with nickel closeouts if the thermal coefficient of expansion is approximately equal to that of half-hard zirconium copper. Mechanical properties, such as yield strength and the modulus of elasticity effect the total strain range; however, the thermal coefficient of expansion is usually the most influential. The mechanical properties have

more of an effect on the fatigue life curve so that the appropriate life curve must be used once the strain range is estimated from figures 8 and 9.

Variations in chamber pressure and coolant inlet pressure also effect the strain range and, hence, life. Small variations of 10 to 15 percent in either pressure should have only a small effect on the total strain range when compared with the effect of the thermally induced mechanical strain at high temperatures. As the hot-gas wall temperature approaches the melting point of the liner material, coolant pressure effects become more predominant because the liner material strength properties are reduced with increasing temperature. Furthermore, as the temperature increases, failure modes other than fatigue could become the primary failure mechanism; that is, cyclic creep, which results from a cyclic mean stress and thermal ratcheting, could accelerate failure.

Lewis Research Center,
National Aeronautics and Space Administration,
Cleveland, Ohio, November 16, 1976,
506-21.

APPENDIX - COMPARISON OF EQUATION-FACTOR TEMPERATURES WITH SINDA TEMPERATURES

In order to establish that equations (2) to (4) were generally acceptable for predicting the radial temperature gradient, temperatures calculated with these equations were compared with those obtained from SINDA. The thermal maps generated with SINDA for the theoretical firing cycle conditions listed in table I were used for comparison. As mentioned previously, equations (2) to (4) provide radial temperature distributions only. Therefore, the temperatures calculated with these equations for each row of structural elements were considered as average temperatures for the appropriate rows. Element temperatures generated with SINDA were averaged for each row and compared with those obtained with the equations.

Figures 12 to 14 show comparisons of element row average temperatures obtained with SINDA and those calculated with the equations. The case numbers on each curve correspond to a cycle condition listed in table I. Notice that data for two liner materials are contained in this table. The thermal properties of these materials are the same so that the thermal maps generated for each case are applicable to thrust chambers with either liner material. The curves in figures 12 and 13 represent the locus of values obtained from equation (2), and the curves in figure 14 represent the locus of values obtained from equations (3) and (4). The symbols associated with each curve are average temperatures that were calculated for each row of the appropriate SINDA thermal map for each cycle condition. It can be seen that the curves represent the average radial temperature distribution quite well. Figure 15 is a comparison of SINDA generated element temperatures and those calculated with the equations and their appropriate weighting factors for the cycle conditions of case 5. The solid line connects the SINDA temperature for each element, and the dashed line connects those calculated by the equation-factor method. The equation-factor curve for the start transient was calculated with equation (2) and the weighting factors of table II. The same curve for the shutdown transient was calculated with equations (3) and (4) and the weighting factors of table III. Both sets of curves compare reasonably well. A structural analysis using the start transient equation factor temperatures showed that the strain error of the maximum strained element was approximately 1 percent when compared with the maximum strained element obtained with SINDA temperatures. Since the shutdown transient curves show better correlation than the start transient curves, the strain error for these thermal conditions should be less. It was concluded then that the equation factor method was satisfactory for generating the thermal maps required for the strain and life curves based on the hot-gas wall temperature and the temperature difference ΔT.

REFERENCES

1. Hanmum, Ned D.; Kasper, Harold J.; and Pavli, Albert J.: Experimental and Theoretical Investigation of Fatigue Life in Several Rocket Thrust Chambers. NASA TM X-73413, 1976.

2. Smith, J. P.: Systems Improved Numerical Differencing Analyzer (SINDA): User's Manual. (TRW-14690-H001-R0-00, TRW Systems Group; NAS9-10435) NASA CR-134271, 1971.

3. Timoshenko, Stephen; and Goodier, J. N.: Theory of Elasticity. 2nd ed., McGraw-Hill Book Co., Inc., 1951.

4. Miller, Roy W.: RETSCP: A Computer Program for Analysis of Rocket Engine Thermal Strains with Cyclic Plasticity. (Atkins and Merrill, Inc.; NAS3-17807) NASA CR-134640, 1974.

5. Miller, Roy W.: Cyclic Fatigue Analysis of Rocket Thrust Chambers. Volume 1: OFHC Copper Chamber Low Cycle Fatigue. (Atkins and Merrill, Inc.; NAS3-17807) NASA CR-134641-vol. -1, 1974.

6. Esposito, John J.; and Zabora, Ronald F.: Thrust Chamber Life Prediction. Volume 1: Mechanical and Physical Properties of High Performance Rocket Nozzle Materials. (D180-18673-1-vol. -1, Boeing Aerospace Co.; NAS3-17838) NASA CR-134806, 1975.

TABLE I. - THEORETICAL FIRING CYCLE CONDITIONS FOR SINDA THERMAL CASES USED TO EVALUATE THE APPLICABILITY OF TEMPERATURE EQUATIONS

[Chamber pressure 4.14 MN/m^2 (600 $lb/in.^2$).]

Case	Liner material	Start type	Cycle period, sec	Coolant flowrate	
				kg/sec	lbm/sec
1	OFHC[a] copper	Slow ramp	8.0	0.94	2.08
2	OFHC copper	Fast ramp	8.0	.94	2.08
3	Zirconium copper	Slow ramp	8.0	.61	1.34
4	Zirconium copper	Fast ramp	7.5	.61	1.34
5	Zirconium copper	Fast ramp	1.6	.61	1.34

[a]Oxygen free, high conductivity.

TABLE II. - MULTIPLYING FACTORS FOR ELEMENT TEMPERATURES AT PEAK ΔT OF START TRANSIENT

$$T_i = KT_{av}; \left(K = \frac{K_1 + K_2 + K_3 + K_4 + K_5}{5}\right)$$

Element	Case 1 K_1	Case 2 K_2	Case 3 K_3	Case 4 K_4	Case 5 K_5	K
1	0.989	0.991	1.000	0.991	1.000	0.994
2	1.000	1.000	1.000	1.000	1.000	1.000
3	1.000	1.000	1.000	1.000	1.000	1.000
4	.861	.869	.929	.892	.918	.894
5	1.039	1.032	1.019	1.029	1.012	1.026
6	1.103	1.096	1.050	1.083	1.049	1.076
7	.990	.990	.991	.992	.992	.991
8	1.009	1.012	1.007	1.008	1.008	1.009
9	.994	.994	.993	.992	.994	.993
10	1.006	1.006	1.006	1.004	1.007	1.006
11	.995	.992	.995	.996	.995	.995
12	1.005	1.006	1.004	1.004	1.003	1.004
13	.999	.999	.998	.997	.997	.998
14	1.001	1.001	1.001	1.003	1.002	1.002
15	1.046	1.063	1.043	1.053	1.054	1.052
16	1.034	1.036	1.031	1.038	1.040	1.036
17	1.004	1.007	1.004	1.004	1.004	1.005
18	.958	.956	.967	.961	.960	.960
19	.950	.937	.953	.943	.941	.945
20	1.039	1.059	1.035	1.042	1.043	1.043
21	1.033	1.051	1.029	1.035	1.037	1.037
22	1.002	1.025	1.010	1.012	1.013	1.012
23	.967	.964	.966	.960	.959	.963
24	.959	.940	.960	.951	.950	.952
25	1.028	1.036	1.027	1.032	1.032	1.031
26	1.023	1.029	1.022	1.026	1.027	1.025
27	1.000	1.000	1.000	1.000	1.000	1.000
28	.978	.971	.979	.975	.974	.975
29	.972	.964	.974	.968	.967	.969
30	1.025	1.032	1.024	1.028	1.024	1.028
31	1.011	1.014	1.011	1.013	1.031	1.012
32	1.000	1.000	1.000	1.000	1.000	1.000
33	.986	.982	.987	.984	.984	.985
34	.977	.971	.979	.975	.973	.983

TABLE III. - ELEMENT TEMPERATURE CONSTANTS

AT PEAK ΔT OF SHUTDOWN TRANSIENT

$[T_i = CT_{av}$ or $T_{av} + C_1.]$

Element	C	$^aC_1$ - ^oR
1	1.000	--
2	1.000	--
3	1.000	--
4	1.013	--
5	.993	--
6	.991	--
7	-----	-1
8	-----	1
9	-----	-1
10	-----	1
11	-----	-1
12	-----	1
13	-----	-1
14	-----	1
15 - 34	1.000	--

[a] C_1 represents the variation in temperature of elements 7 to 14 from the average temperature calculated with eq. (4).

TABLE IV. - MAXIMUM STRAIN RANGE VALUES

Firing cycle case from table I	Total strain range with residual strains, %	Strain range[a], %		
		Start	Shutdown	Total
1	2.22	2.08	0.23	2.31
2	1.95	1.70	.20	1.90
3	2.35	2.22	.23	2.45
4	2.44	2.20	.29	2.49
5	2.31	2.21	.21	2.42

[a] From figs. 8 and 9.

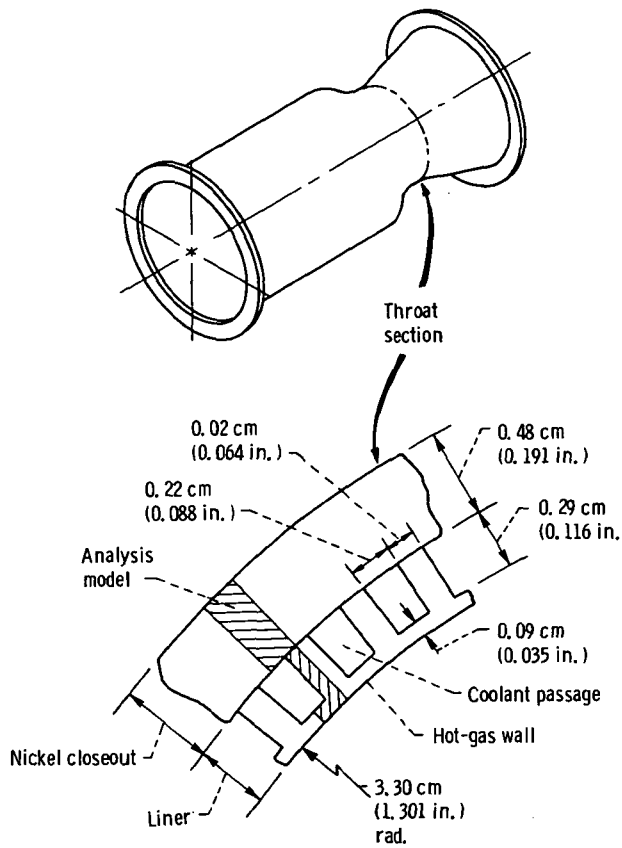

Figure 1. - Fatigue life test thrust chamber.

Location	K	°R	Location	K	°R
1	696	1253	47	249	448
2	700	1260	48	233	420
3	706	1271	49	205	369
4	715	1287	50	183	330
5	724	1304	51	167	301
6	732	1317	52	161	289
7	736	1324	53	209	376
8	663	1193	54	197	354
9	668	1203	55	174	314
10	676	1217	56	157	283
11	688	1239	57	154	277
12	700	1261	58	149	269
13	709	1276	59	142	255
14	713	1284	60	135	243
15	624	1123	61	101	181
16	630	1134	62	99	179
17	641	1153	63	98	177
18	664	1196	64	97	174
19	682	1227	65	63	114
20	692	1245	66	63	114
21	697	1254	67	63	114
22	567	1020	68	63	113
23	567	1021	1069	710	1278
24	566	1018	1071	714	1285
25	502	904	1073	719	1295
26	501	902	1075	728	1311
27	498	896	1077	738	1328
28	448	806	1079	745	1341
29	446	803	1081	749	1348
30	443	798	1083	691	1244
31	402	724	1085	686	1235
32	400	721	1087	676	1217
33	398	716	1089	659	1187
34	365	657	1091	563	1013
35	363	653	1093	496	892
36	361	649	1095	441	794
37	335	603	1097	396	713
38	331	596	1099	358	645
39	328	590	1101	326	587
40	276	497	1103	211	380
41	284	511	1105	180	324
42	269	485	1107	162	292
43	217	390	1109	155	279
44	184	332	2001	3413	6143
45	167	300	2002	45	81
46	159	286			

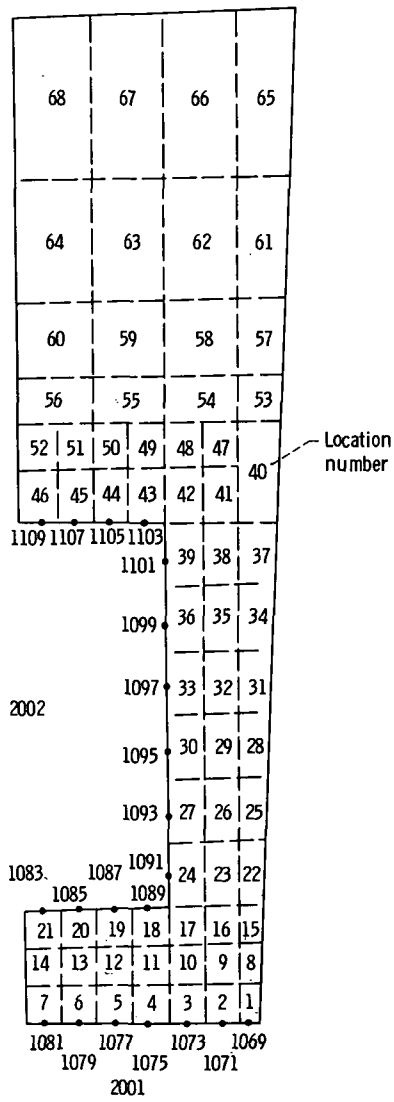

Figure 2. - Typical SINDA model and temperatures for start transient of case 5 of table I.

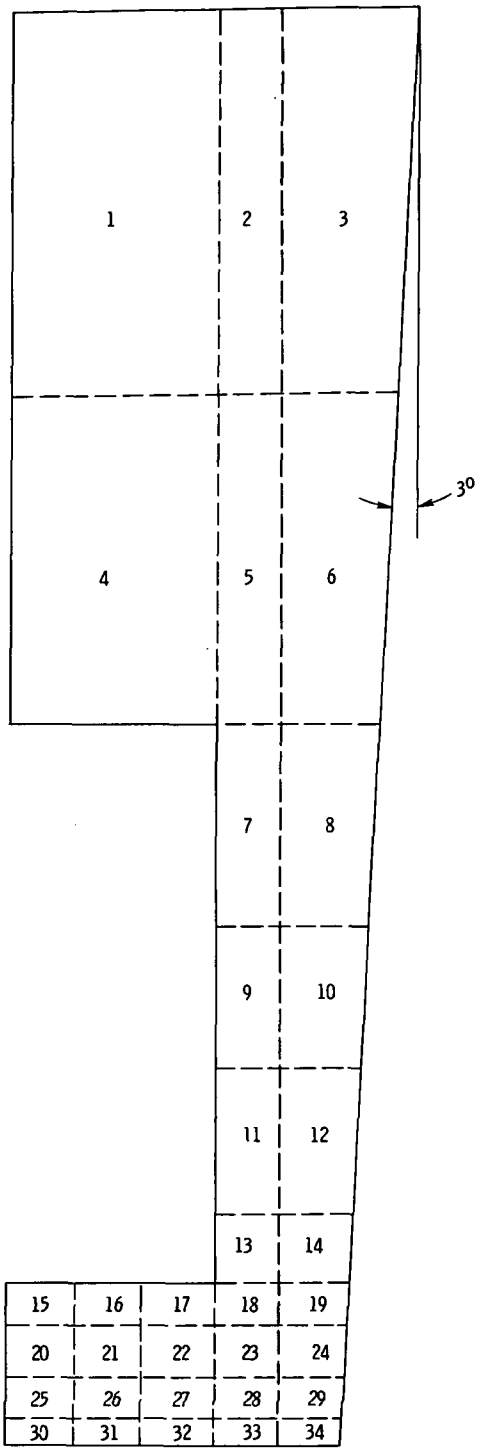

Figure 3. - Structural model with element numbers.

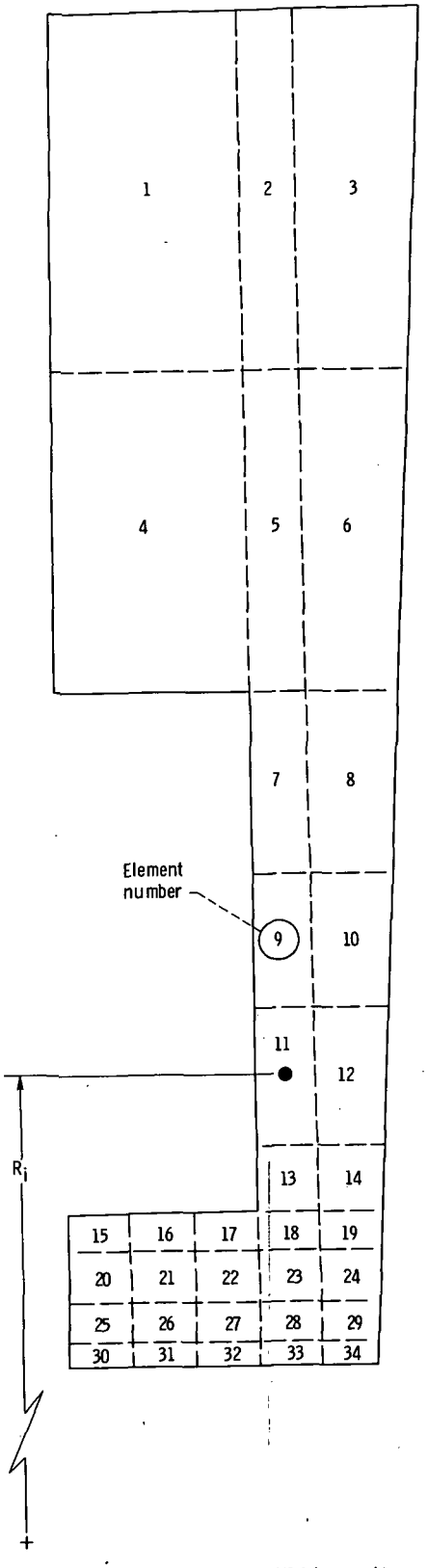

Element	Element radius, r_i		Temperature	
	cm	in.	K	°R
1	4.03	1.585	63	113
2	4.03	1.585	63	114
3	4.03	1.585	63	114
4	3.78	1.490	165	298
5	3.78	1.490	197	354
6	3.78	1.490	209	376
7	3.63	1.430	345	620
8	3.63	1.430	350	630
9	3.54	1.395	398	716
10	3.54	1.395	402	724
11	3.47	1.365	498	896
12	3.47	1.365	502	904
13	3.41	1.3425	566	1018
14	3.41	1.3425	566	1020
15	3.38	1.3325	696	1254
16	3.38	1.3325	686	1236
17	3.38	1.3325	664	1196
18	3.38	1.3325	636	1144
19	3.38	1.3325	624	1123
20	3.36	1.3225	705	1269
21	3.36	1.3225	700	1261
22	3.36	1.3225	685	1233
23	3.36	1.3225	650	1169
24	3.36	1.3225	644	1158
25	3.33	1.3125	724	1304
26	3.33	1.3125	720	1297
27	3.33	1.3125	702	1263
28	3.33	1.3125	684	1232
29	3.33	1.3125	679	1223
30	3.31	1.3025	749	1348
31	3.31	1.3025	738	1328
32	3.31	1.3025	728	1311
33	3.31	1.3025	716	1290
34	3.31	1.3025	710	1278

Figure 4. - SINDA temperatures at structural element centers for case 5.

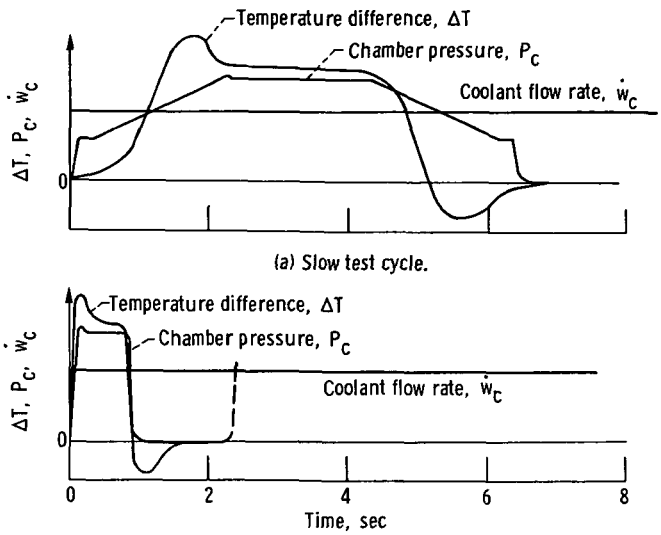

Figure 5. - Schematic representation of relation of three cycle parameters during two different firing cycles.

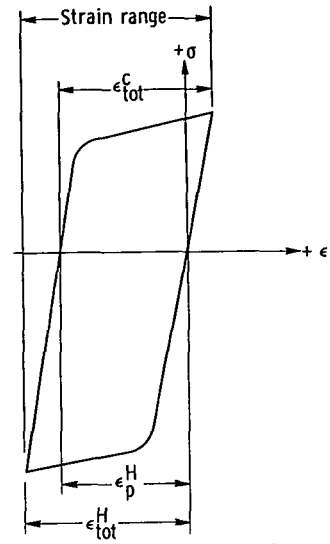

Strain range = $\epsilon^H_{tot} + \left(\epsilon^c_{tot} - \epsilon^H_p\right)$

where

ϵ^H_{tot} = total strain during start

ϵ^H_p = plastic strain during start

ϵ^c_{tot} = total strain during shutdown

Figure 6. - Theoretical stress-strain hysteresis loop.

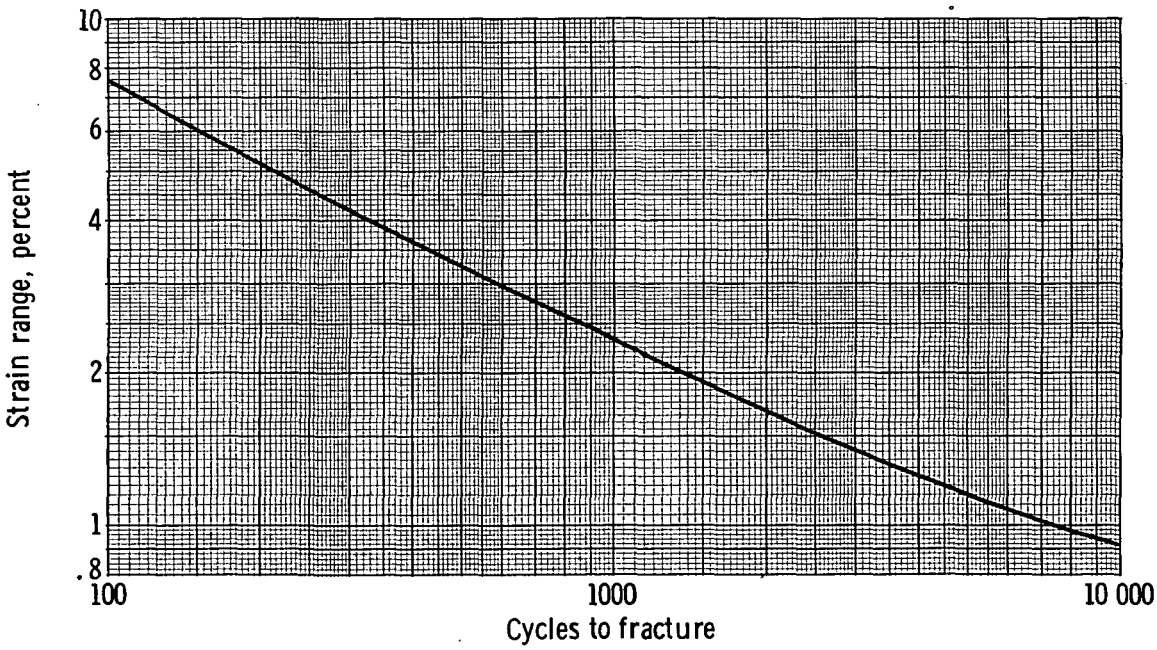

Figure 7. - Typical low-cycle fatigue life of half hard Zr-Cu.

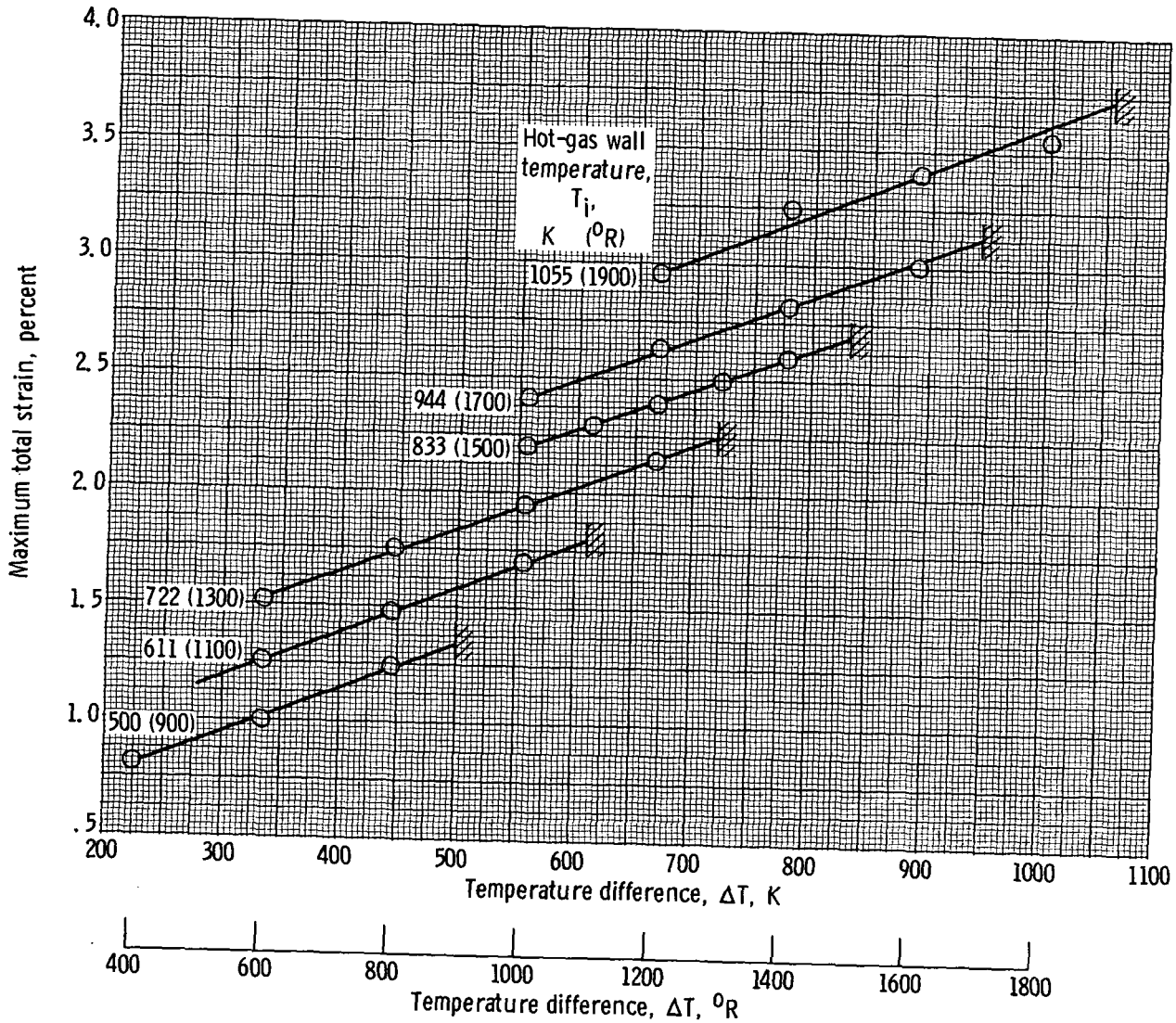

Figure 8. - Effect of hot-gas wall temperature and ΔT on total strain of maximum strained element at time of peak ΔT during start transient.

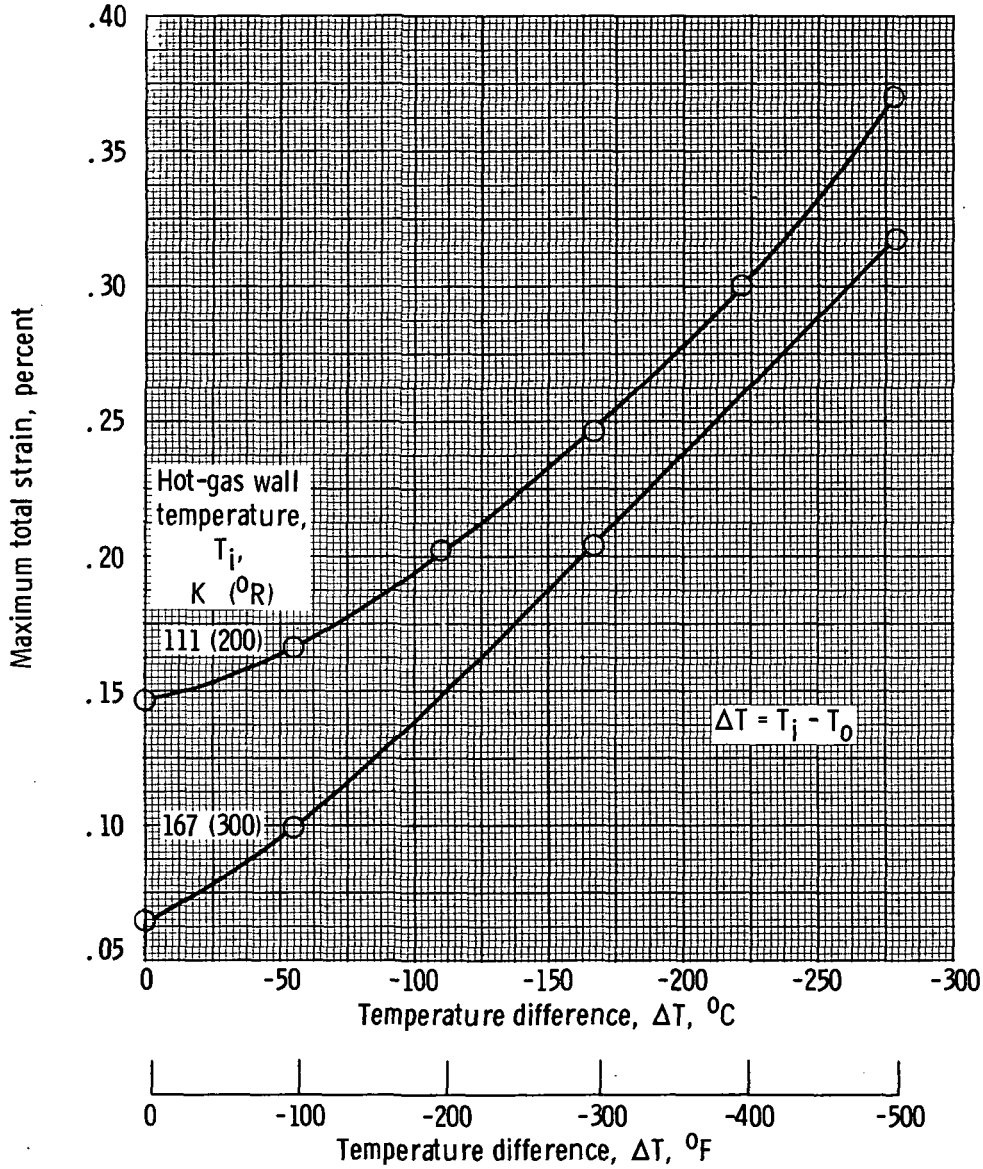

Figure 9. - Effect of hot-gas wall temperature and ΔT on total strain of maximum strained element at time of peak ΔT during shutdown transient.

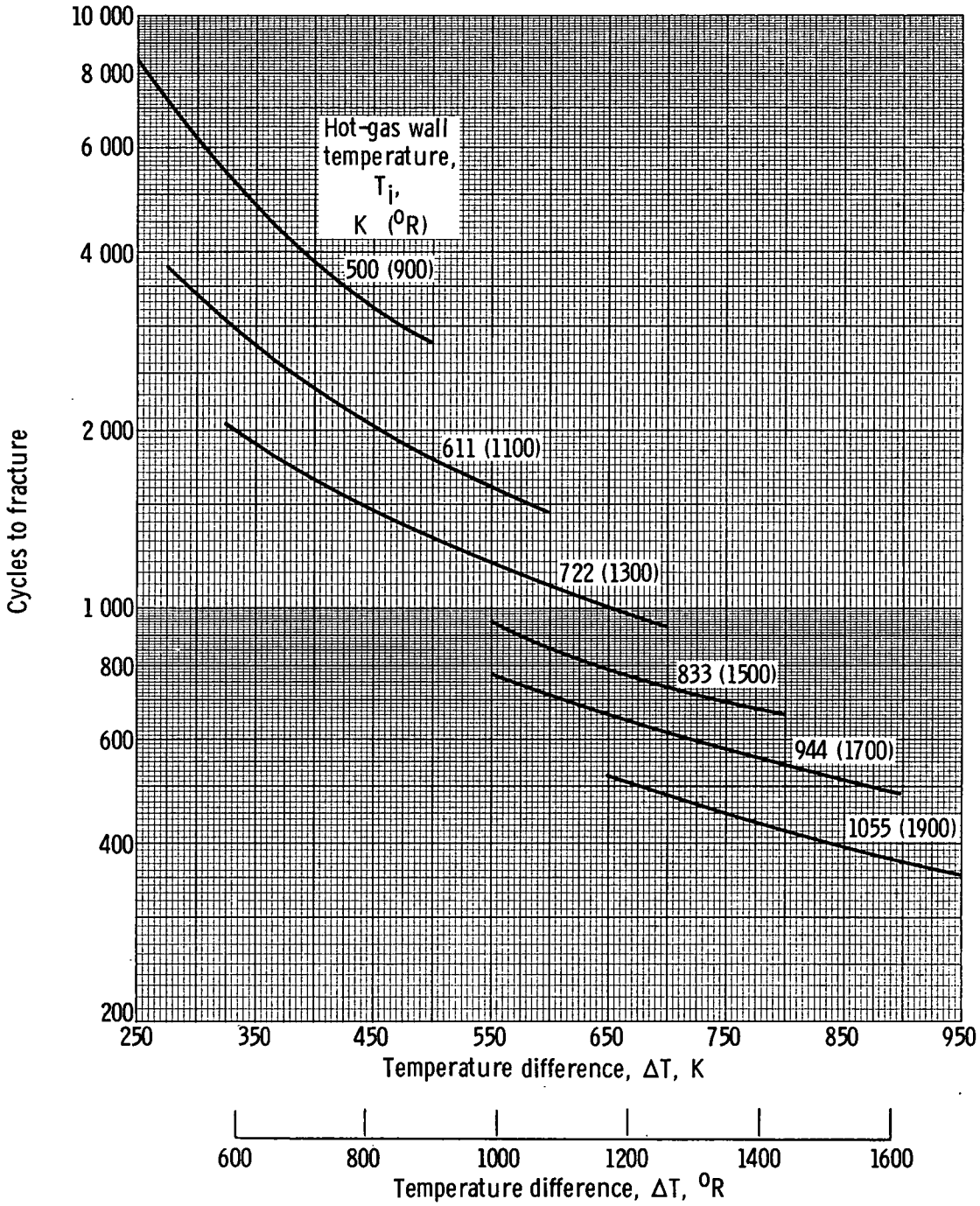

Figure 10. - Effect of wall temperature and ΔT on life of thrust chamber with half-hard zirconium-copper liner and nickel closeout.

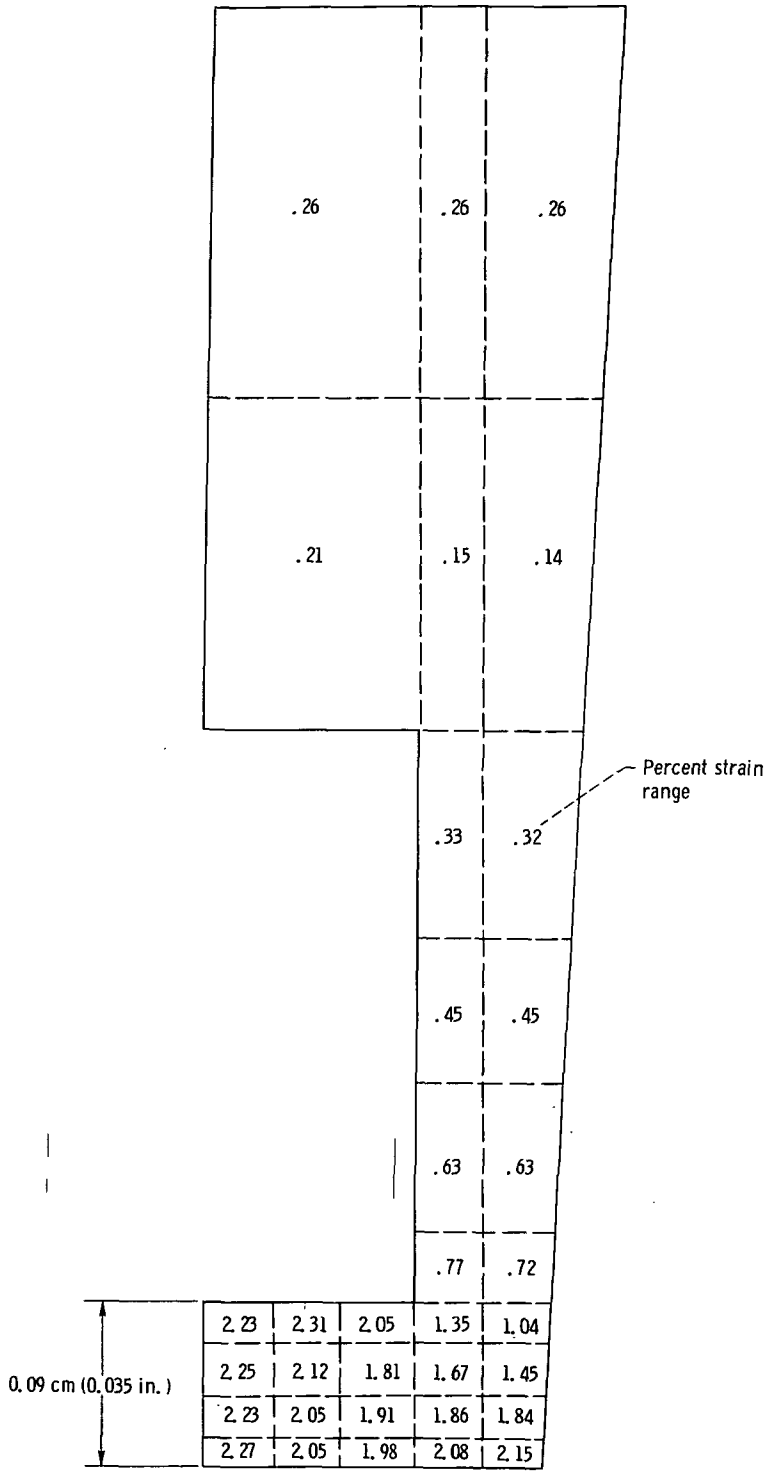

Figure 11. - Strain range distribution for case 5 of table I.

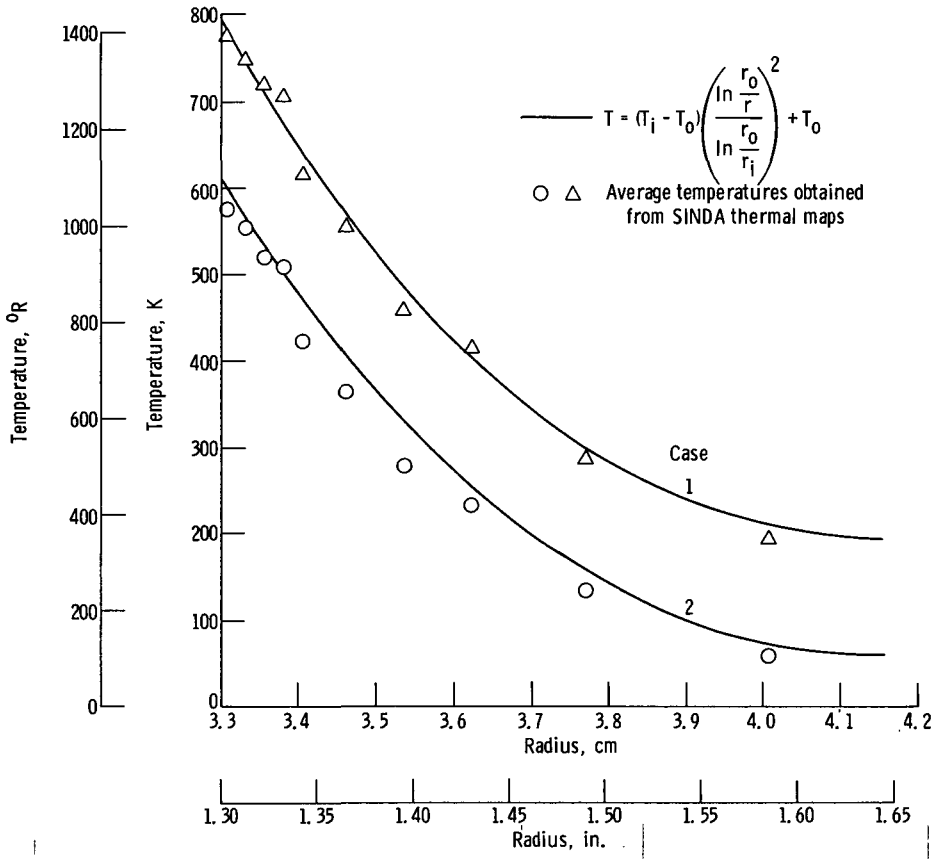

Figure 12. - Comparison of element row average temperatures obtained with SINDA and those calculated with equation (2) for the start transients of cases 1 and 2.

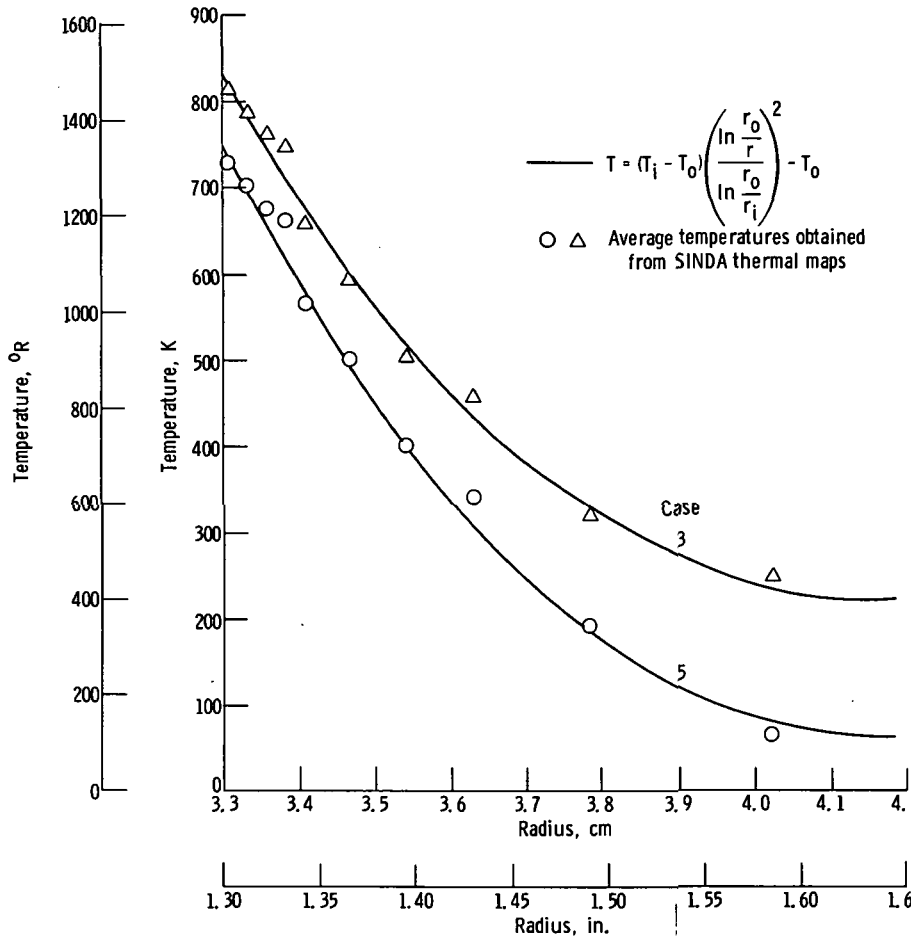

Figure 13. - Comparison of element row average temperatures obtained with SINDA and those calculated with equation (2) for the start transients of cases 3 and 5.

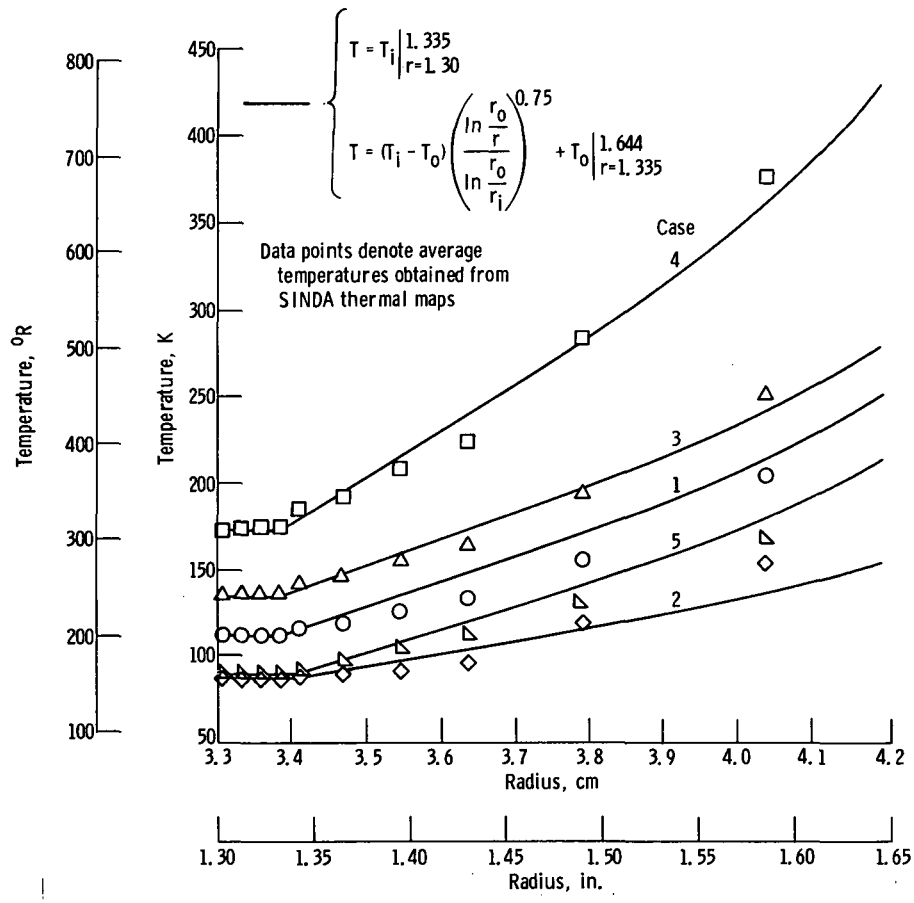

Figure 14. - Comparison of element row average temperatures obtained with SINDA and those calculated with equations (2) and (3) for the shutdown transients of cases 1 to 5.

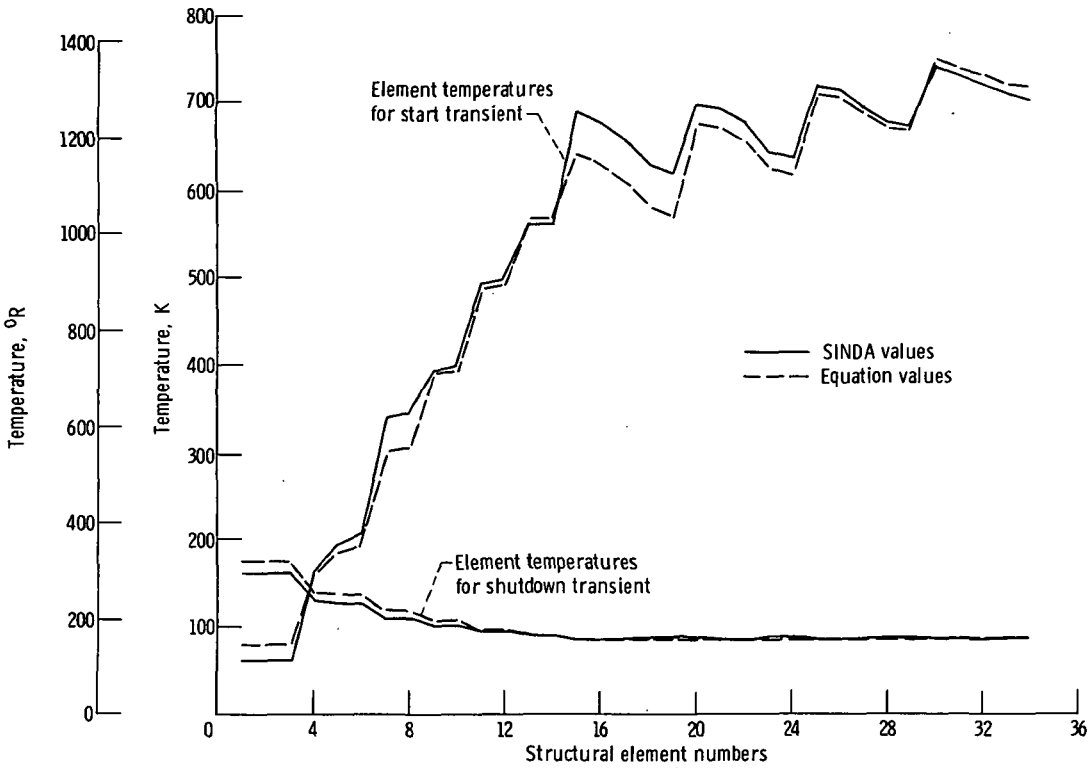

Figure 15. - Comparison of individual element temperatures obtained with SINDA and those calculated by equation-factor method for case 5.

NATIONAL AERONAUTICS AND SPACE ADMINISTRATION
WASHINGTON, D.C. 20546

OFFICIAL BUSINESS
PENALTY FOR PRIVATE USE $300

SPECIAL FOURTH-CLASS RATE
BOOK

POSTAGE AND FEES PAID
NATIONAL AERONAUTICS AND
SPACE ADMINISTRATION
451

U.S.MAIL

POSTMASTER: If Undeliverable (Section 158 Postal Manual) Do Not Return

"The aeronautical and space activities of the United States shall be conducted so as to contribute . . . to the expansion of human knowledge of phenomena in the atmosphere and space. The Administration shall provide for the widest practicable and appropriate dissemination of information concerning its activities and the results thereof."

—NATIONAL AERONAUTICS AND SPACE ACT OF 1958

NASA SCIENTIFIC AND TECHNICAL PUBLICATIONS

TECHNICAL REPORTS: Scientific and technical information considered important, complete, and a lasting contribution to existing knowledge.

TECHNICAL NOTES: Information less broad in scope but nevertheless of importance as a contribution to existing knowledge.

TECHNICAL MEMORANDUMS: Information receiving limited distribution because of preliminary data, security classification, or other reasons. Also includes conference proceedings with either limited or unlimited distribution.

CONTRACTOR REPORTS: Scientific and technical information generated under a NASA contract or grant and considered an important contribution to existing knowledge.

TECHNICAL TRANSLATIONS: Information published in a foreign language considered to merit NASA distribution in English.

SPECIAL PUBLICATIONS: Information derived from or of value to NASA activities. Publications include final reports of major projects, monographs, data compilations, handbooks, sourcebooks, and special bibliographies.

TECHNOLOGY UTILIZATION PUBLICATIONS: Information on technology used by NASA that may be of particular interest in commercial and other non-aerospace applications. Publications include Tech Briefs, Technology Utilization Reports and Technology Surveys.

Details on the availability of these publications may be obtained from:

SCIENTIFIC AND TECHNICAL INFORMATION OFFICE

NATIONAL AERONAUTICS AND SPACE ADMINISTRATION

Washington, D.C. 20546